Asian Journal of Chemistry; Vol. 33, No. 9 (2021), 2043-2048

ASIAN JOURNAL OF CHEMISTRY

https://doi.org/10.14233/ajchem.2021.23289

Role of Cationic and Anionic Dopants on the Structural, Morphological, Optical and Magnetic Properties of Lead Oxide Nanocrystals Prepared by Solvothermal Method

N. SARASWATHI[1] and K.J. ABHIRAMA[2,*]

[1]Department of Physics, Arignar Anna College, Aralvaimozhi-629301, India
[2]Department of Physics, Sree Devi Kumari Women's College, Kuzhithurai-629163, India

*Corresponding author: E-mail: abhiramathampi87@gmail.com

Received: 1 May 2021; *Accepted*: 11 June 2021; *Published online*: 20 August 2021; AJC-20462

A facile and simple microwave assisted solvothermal technique was adopted for the synthesis of undoped and doped (Mn^{2+}, S^{2-}) lead oxide nanoparticles. Thermogravimetric analysis and differential thermal analysis were carried out to realize the thermal behaviour of PbO nanoparticles. The synthesized nanoparticles were annealed at about 400 ºC. The calcined samples were characterized by powder X-ray diffraction, SEM, EDX, UV spectroscopic analysis and VSM measurement. The diffraction patterns of the prepared nanoparticles showed the formation of an orthorhombic phase of lead oxide. All the samples were in nano- regime with an average grain size of 22-26 nm. Spherical morphology of the samples was revealed in the SEM micrographs. EDX pattern confirmed the presence of cationic and anionic dopants. The band gap energy values range from 4.2 to 5.6 eV. The VSM measurement revealed that the sample has weak ferromagnetic nature.

Keywords: Microwave, Solvothermal, Lead oxide, Orthorhombic, Annealed.

INTRODUCTION

Metal oxide nanomaterials show metallic, semiconductor and also insulator characteristics depending on the dopants included as well as the size of the particles. These interesting metal oxide nanomaterials find application in fabrication of piezoelectric devices, microelectronic circuits, sensors, fuel cells, anticorrosion coatings, *etc.* [1-7]. They exhibit distinct chemical and physical properties as a result of their quantum confinement in the nano-regime and high density of corner or edge surface sites. Unlike bulk oxide materials that are stable with well-defined crystallographic structures, the nano dimensions of the bulk materials modifies cell parameters and crystal structure [8-11]. Metal oxide-cellulose nanocomposites are found very effective in removing toxic materials from impure water [12].

Lead(II) oxide is a semiconductor material with numerous applications. It is an attractive material because of its several phases such as Pb_2O, Pb_2O_3 and Pb_3O_4 [13]. PbO finds place in industries as material for storage batteries, pigments, gas sensors and in paints [14,15]. The two crystalline forms of PbO are tetragonal (litharge α-PbO form) and orthorhombic (massicot β-PbO form). The former one is stable at low temperatures and the latter one is stable at high temperatures [16]. This interesting nanocrystal material is synthesized commonly by hydrothermal method, thermal decomposition, chemical precipitation, electron beam irradiation and sonochemical synthesis [17-22]. Hashim *et al.* [23] synthesized carboxymethyl cellulose-polyvinyl/pyrrdidone-polyvinyl alcohol/lead oxide nanoparticles for gamma applications. Thermal decomposition method was followed by Varzdar *et al.* [13] for the synthesis of a 2D lead oxide coordination polymer. High temperature oxidation-evaporation and condensation technique was adopted by Zhan *et al.* [24] for the preparation of lead oxide nanoparticles from waste electric and electronic equipments. Ghaedi *et al.* [22] employs lead oxide nanoparticles loaded activated carbon synthesized by sonochemical method for the removal of methyl orange from aqueous solutions.

Cadmium doped PbO nanoparticle using solvothermal technique was synthesized by Rejith & Sudha [25] with a particle size of 74 nm. Pure and Zn doped PbO nanostructure was synthesized by Taunk *et al.* [26] *via* chemical route. Optical

band gap of 5.17 and 5.5eV was reported for pure and doped PbO samples. Literature shows that only metals were used as dopants in the study of lead oxide nanoparticles. In the present work, synthesis of undoped, cationic and anionic doped lead oxide nanocrystals by a simple, cost effective and novel microwave assisted solvothermal technique using simple domestic microwave oven is reported.

EXPERIMENTAL

All the reagents and solvents required for the synthesis of lead oxide nanoparticles are commercially available and are used as received.

Synthesis of PbO nanoparticles: Undoped lead oxide nanocrystals were prepared using lead acetate, urea and ethylene glycol. Lead acetate and urea were taken in the molecular ratio 1:3 and dissolved in 100 mL ethylene glycol (solvent) to prepare PbO sample. The Mn^{2+} doped PbO samples (2.5 and 5 wt.% added) were prepared by using manganese acetate with the above precursors used for the preparation of undoped samples. The S^{2-} doped samples (2.5 and 5 wt.% added) were prepared using thiourea with the basic precursors needed for the undoped samples. The solutions with the respective precursors were stirred well with a magnetic stirrer until the materials dissolved completely. The dissolved solution was kept in a domestic microwave oven (Onida model-Power Solo 20) operated with a frequency of 2.45 GHz and power 800 Watts). Microwave irradiation was carried out till the solvent evaporated completely and a colloidal precipitate was obtained. The precipitate was washed for about six times with double distilled water to remove the water soluble impurities and then about three times with acetone to remove the organic impurities. The washed samples were dried in atmospheric air and collected as yield.

Analysis: The TGA and DTA analysis were carried out for undoped PbO nanoparticles with NETZSCH STA 409 C/CD. Then the prepared samples were calcined at 400 ºC for about 1 h. The annealed samples were characterized by powder X-ray diffraction analysis using X'Pert Pro-Panalytic instrument and UV-Vis NIR absorption spectroscopic analysis by Shimadzu UV-2400 PC spectrophotometer. The magnetic measurements were carried out using Lakeshore, USA, model 7407 vibrating sample magnetometer.

RESULTS AND DISCUSSION

TG/DTA analysis: To obtain the appropriate annealing temperature and also to improve the phase purity and ordering of the samples, thermal analysis was performed using TGA and DTA analysis in the temperature range 20-1000 ºC. The TGA and DTA patterns are shown in Fig. 1. Dehydration and ejection of absorbed water was observed in the DTA curve. TGA curve shows that the prepared sample is thermally stable up to 260 ºC. Weight loss of 13% was observed in the temperature range 260-380 ºC and it is because of the phase change of lead oxide from α-PbO to β-PbO. After 380 ºC, the sample is stable. So we fixed the annealing temperature as 400 ºC and annealed all the prepared samples at this temperature for about 1 h.

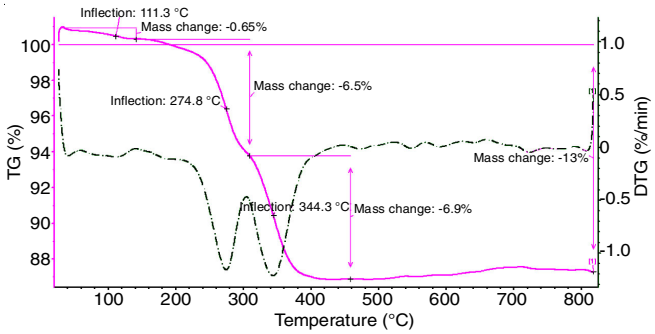

Fig. 1. TGA/DTA analysis curves for unannealed PbO nanoparticles

Powder-XRD analysis: The PXRD patterns of undoped and doped PbO nanoparticles are shown in Fig. 2. The diffraction peaks obtained reveal that the prepared samples are β-PbO with orthorhombic structure and it matches well with JCPDS card No. 03-0610.

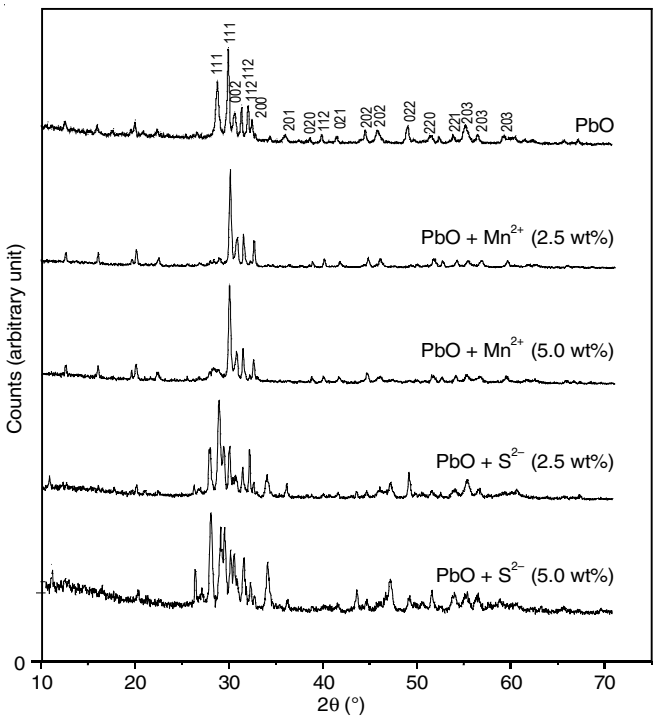

Fig. 2. Indexed PXRD patterns of undoped and doped PbO nanparticles

The average grain size of the particle was calculated using the Scherrer equation:

$$D = \frac{K\lambda}{\beta\cos\theta}$$

where λ is the wavelength of incident beam, β is the full width at half maximum of the diffraction peak (in radian), θ is the diffraction angle and K is the Scherer's constant (0.9).

All the prepared PbO samples are in the nanoscale with average grain size ranging from 22-26 nm. The calculated lattice parameter (a, b, c) values are tabulated in Table-1. Salavati-Niasari *et al.* [27] synthesized PbO nanocrystals by thermal decomposition route with an average grain size of 36 nm. The broadening of peaks in the PXRD pattern is mainly due to the

TABLE-1
AVERAGE GRAIN SIZES AND LATTICE PARAMETERS FOR UNDOPED AND DOPED PbO NANOPARTICLES

System (with expected composition)	Average grain size (nm) (± 5% error)	Lattice parameters		
		a (Å)	b (Å)	c (Å)
PbO	22.96	5.5673	5.9041	4.7570
PbO + 2.5 wt % Mn^{2+}	26.06	5.5572	5.8452	4.7342
PbO + 5.0 wt % Mn^{2+}	21.67	5.5387	5.9159	4.6932
PbO + 2.5 wt % S^{2-}	22.70	5.5033	5.9343	4.8344
PbO + 5.0 wt % S^{2-}	22.09	5.5281	5.9382	4.7130

formation of nanostructured material [28]. The variation of average grain size values from that of undoped PbO is due to the incorporation of dopants on the host matrix.

Morphology: The SEM micrographs recorded with 5,000x magnification are shown in Fig. 3. The SEM images show that the prepared nanoparticles were agglomerated and spherical shaped cluster like patterns. The interface between the precursors and the solvent (ethylene glycol) is capable of controlling nucleation and the growth process. Also the particle size as well as distribution of nanoparticles plays a vital role in the relative rate of nucleation and agglomeration of particles [29]. Increase in agglomeration was observed in the doped samples when compared to undoped PbO. This is mainly due to inclusion of dopants on the host matrix.

Energy dispersive X-ray spectroscopic analysis was carried out for the identification and quantification of elemental compositions in the sample [30]. EDX patterns (Fig. 4) confirms the insertion of dopants into the pure samples. The EDX spectral analysis of the sample clearly indicates that there are no other impurities in the sample prepared by this method. This result confirms that all the prepared samples have high phase purity and crystallinity. The elemental compositions in the sample is shown in Table-2.

TABLE-2
MATERIAL COMPOSITION (ATOMIC %) OBTAINED USING EDX

System (with expected composition)	Material composition (atomic %)			
	Lead	Oxide	Manganese	Sulphur
PbO	31.91	68.09	–	–
PbO + 2.5 wt % Mn^{2+}	31.21	68.18	0.61	–
PbO + 5 wt % Mn^{2+}	29.16	69.48	1.36	–
PbO + 2.5 wt % S^{2-}	30.07	68.50	–	1.43
PbO + 5 wt % S^{2-}	26.55	71.58	–	1.87

UV analysis: The nature of the chemical compositions can cause major differences in the optical properties of the nanostructured marterials. Low absorbance in the visible region was observed in the UV-Vis spectra. Tauc plot was drawn to obtain the band gap energies of the samples and shown as inset graphs in Fig. 5.

The plots specify the presence of a direct optical band gap and the band gap energy value was found for each sample by extrapolating the curve drawn near the absorption edge. The optical band gap energy values obtained for the prepared samples are shown in Table-3. The values range from 4.2 to 5.6 eV. Direct band gap value of 5.2 eV was reported by Thielsch *et al.* [31]. The calculated values are much higher than that reported (1.9 eV) for PbO nanocrystals [32] and also higher

TABLE-3
BAND GAP ENERGY VALUES FOR UNDOPED AND DOPED PbO NANOCRYSTALS

Sample (with estimated composition)	E_g (eV)
PbO	5.343
PbO + 2.5 wt % Mn^{2+}	4.212
PbO + 5 wt % Mn^{2+}	5.641
PbO + 2.5 wt % S^{2-}	5.012
PbO + 5 wt % S^{2-}	5.566

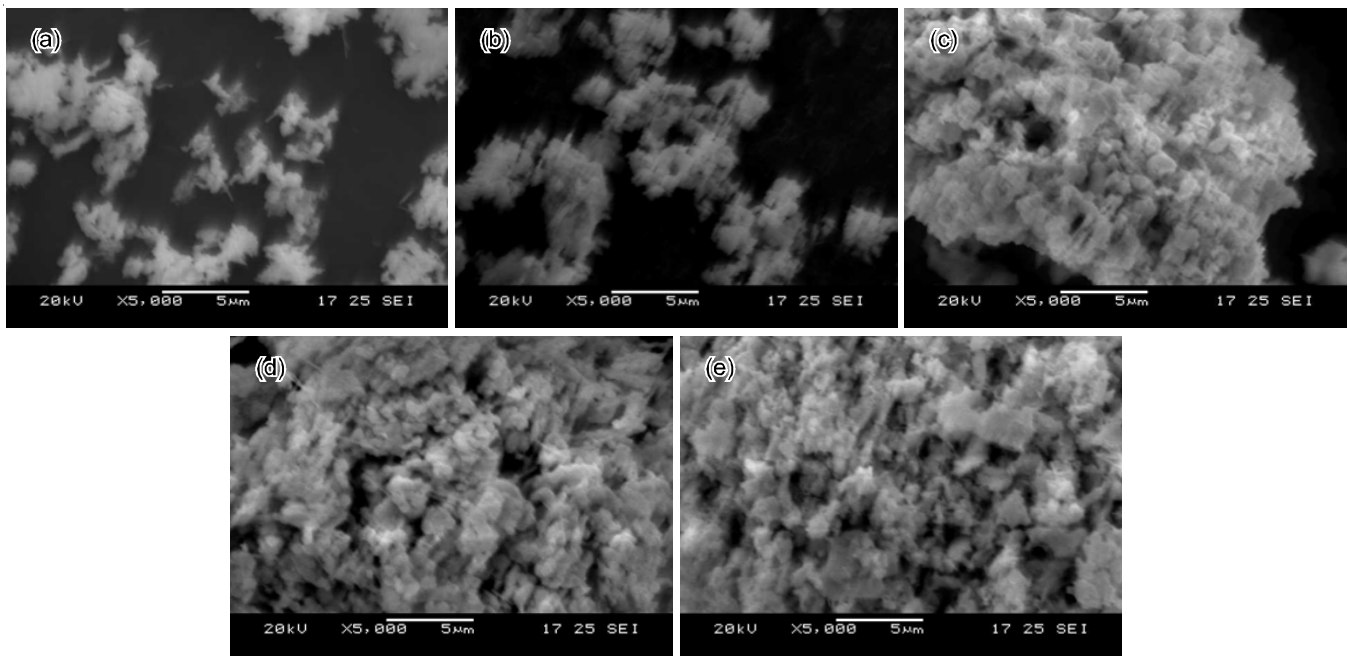

Fig 3. SEM image of (a) PbO nanoparticles, (b) PbO + 2.5 wt % Mn^{2+} nanoparticles, (c) PbO + 5.0 wt % Mn^{2+} nanoparticles, (d) PbO + 2.5 wt % S^{2-} nanoparticles, (e) PbO + 5.0 wt % S^{2-} nanoparticles

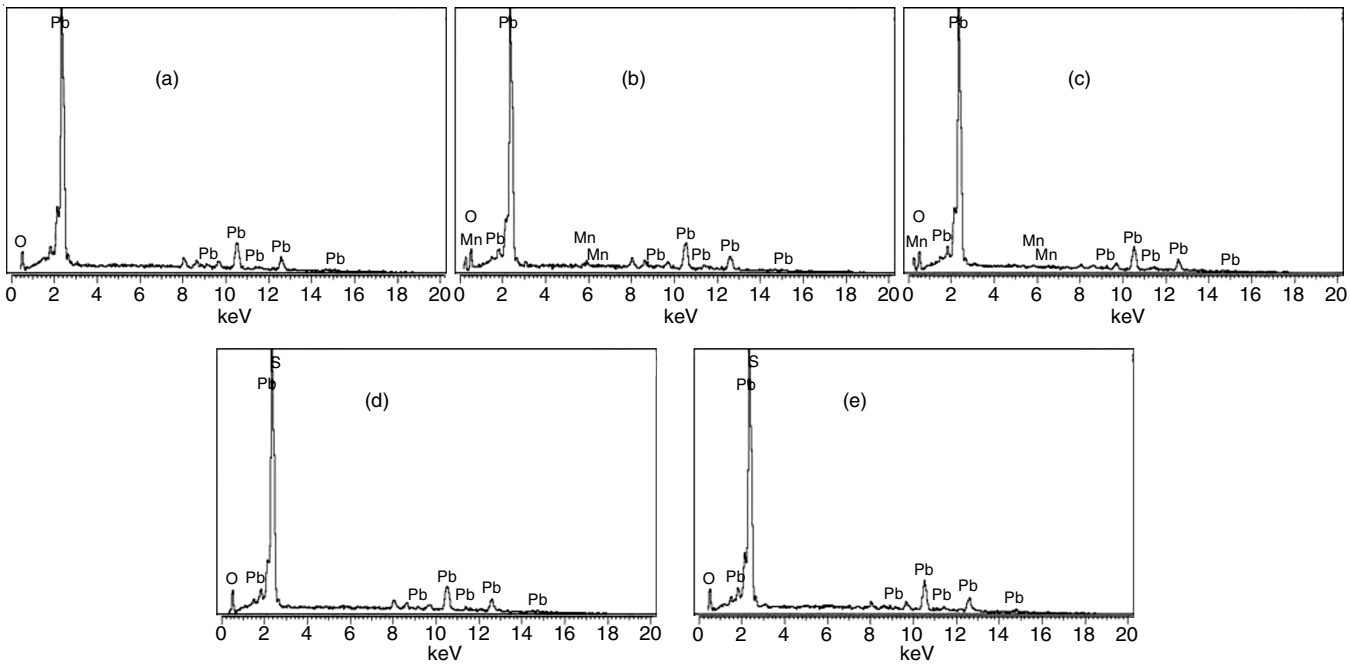

Fig. 4 EDX pattern of (a) PbO nanoparticles, (b) PbO + 2.5 wt % Mn^{2+} nanoparticles, (c) PbO + 5.0 wt % Mn^{2+} nanoparticles, (d) PbO + 2.5 wt % S^{2-} nanoparticles, (e) PbO + 5.0 wt % S^{2-} nanoparticles

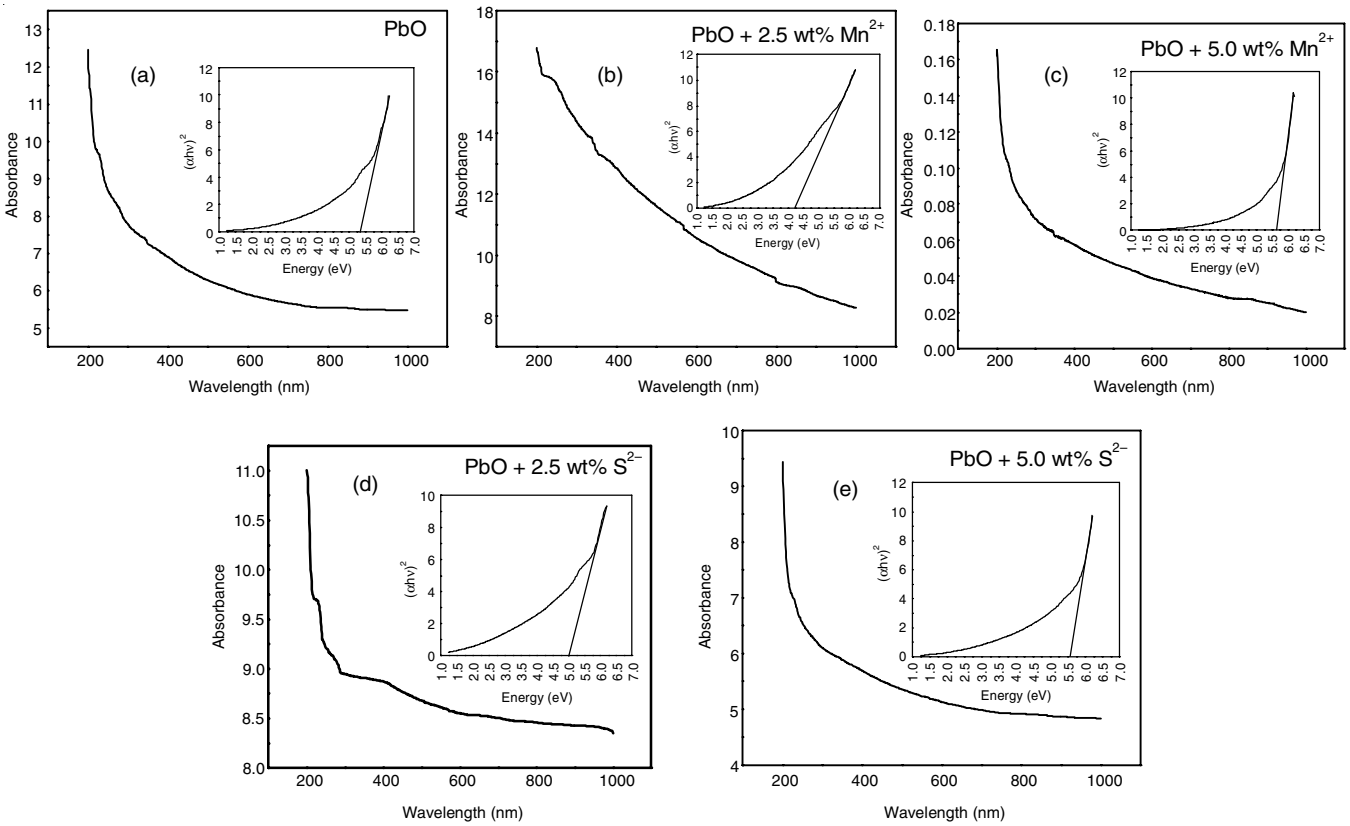

Fig. 5. UV-Vis-NIR spectrum of (a) PbO nanocrystals, (b) PbO + 2.5 wt % Mn^{2+} nanocrystals, (c) PbO + 5.0 wt % Mn^{2+} nanocrystals, (d) PbO + 2.5 wt % S^{2-} nanocrystals, (e) PbO + 5.0 wt % S^{2-} nanocrystals

than that of bulk PbO crystal indicating clearly a blue shift in the absorption wavelengths.

The obtained band gap energies were related with the average grain sizes calculated from the PXRD patterns. It is inferred that the band gap energy value depends on the grain size. The increase in band gap energy for most of the prepared PbO samples was mainly due to decrease in the grain size [33]. This increase in the band gap energy may be due to the quantum confinement in the nanocrystal samples at that particular dopant concentration.

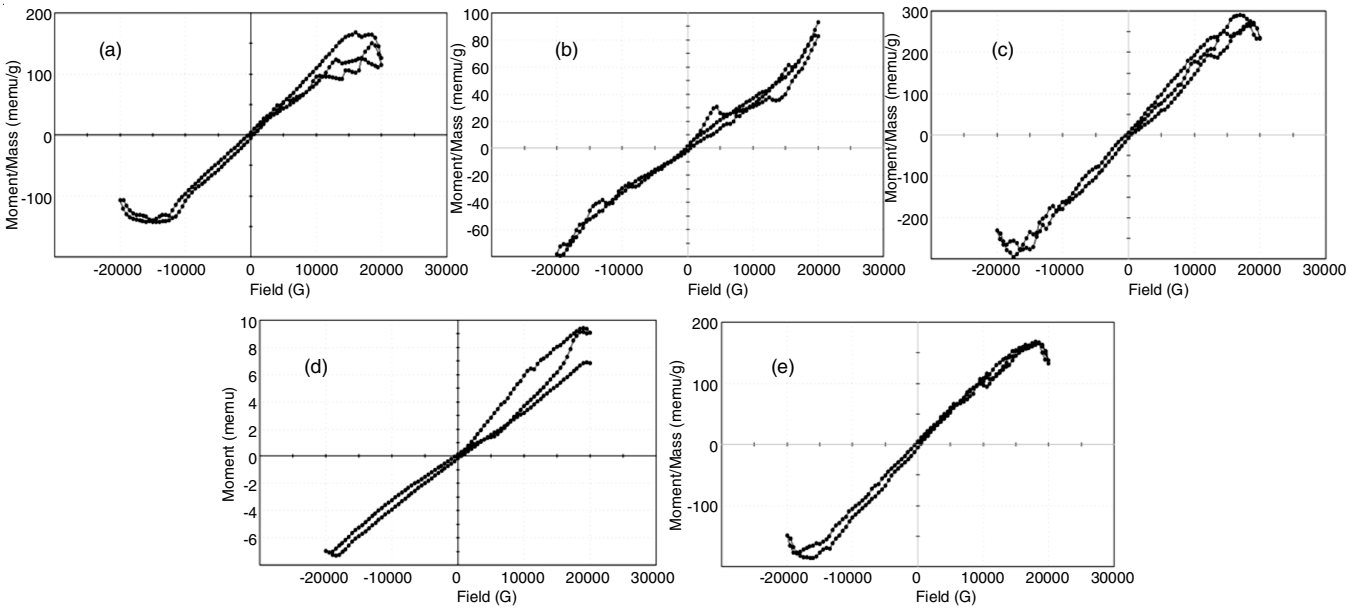

Fig. 6. Magnetization curve of (a) PbO nanocrystals, (b) PbO + 2.5 wt % Mn^{2+} nanocrystals, (c) PbO + 5.0 wt % Mn^{2+} nanocrystals, (d) PbO + 2.5 wt % S^{2-} nanocrystals, (e) PbO + 5.0 wt % S^{2-} nanocrystals

TABLE-4
RESULTS OBTAINED FROM VSM MEASUREMENTS FOR PURE AND DOPED (Mn^{2+} AND S^{2-}) PbO NANOCRYSTALS

System (with expected composition)	Coercivity, H_c (G)	Retentivity, M_r (× 10^{-6} emu)	Magnetization, M_s (× 10^{-3} emu)	Squareness ratio, M_r/M_s (×10^{-3})
PbO	382.21	4.4998	0.1556	28.910
PbO + 2.5 wt % Mn^{2+}	388.00	1.8664	0.0863	21.620
PbO + 5 wt % Mn^{2+}	384.57	6.5751	0.2941	22.360
PbO + 2.5 wt % S^{2-}	395.45	149.86	8.3600	17.920
PbO + 5 wt % S^{2-}	390.79	5.1294	0.1771	28.970

VSM measurement: The M-H behaviour of the annealed samples was studied at room temperature using a vibrating sample magnetometer. The M-H plots obtained are shown in Fig. 6 and the magnetic parameters are given in Table-4. The M-H curves of the samples show a small magnetic hysteresis loop, which indicates that the samples exhibit a weak ferromagnetic nature. Hysteresis with related ferromagnetism in ZnO nanocrystals doped with Cr^{3+} was reported by Chu *et al.* [34]. The coercive field (H_c) or coercivity is defined as the field necessary to reduce the net moment to zero. The *y*-intercept of descending curve is saturation remanence (M_r) or retentivity. The coercivity is minimum in the case of pure PbO nanocrystal. Retentivity and magnetization are maximum in the case of PbO doped with 2.5 wt.% S^{2-}. The calculated squareness ratio is minimum in the case of 2.5 wt.% S^{2-} doped sample. The anionic (sulphur) doping makes PbO a better magnetic semiconductor.

Conclusion

Microwave assisted solvothermal technique using a domestic microwave oven was an effective, simple and convenient method for the preparation of undoped and doped (Mn^{2+} and S^{2-}) PbO nanoparticles. From thermogravimetric analysis, the calcination temperature was fixed as 400 ºC. The prepared samples were calcined at that particular temperature for about 1 h to improve the phase purity. The PXRD measurements were done for all the annealed samples. Broadening of peaks in the PXRD pattern shows that the samples are in nano-scale. Also the pattern confirmed that PbO nanoparticles have orthorhombic structures with β-PbO phase. The grain size was found to increase in the case of 2.5 wt.% Mn^{2+} doped sample unlike others. This may be due to selective inclusion of the dopant at that particular concentration which led to an increase in band gap energy also. SEM micro-graphs showed the agglomerated and spherical morphology. The presences of cationic and anionic dopants in the doped samples were confirmed using the EDX patterns. The UV-vis spectra showed a low absorbance in the visible region. The calculated band gap values were higher than that of bulk indi-cating a blue shift with absorption wavelength. The M-H curves plotted for the samples show a weak ferromagnetic nature.

CONFLICT OF INTEREST

The authors declare that there is no conflict of interests regarding the publication of this article.

REFERENCES

1. A. Rastogi, M. Zivcak, O. Sytar, H.M. Kalaji, X. He, S. Mbarki and M. Brestic, *Front. Chem.*, **5**, 78 (2017); https://doi.org/10.3389/fchem.2017.00078
2. M.S. Chavali and M.P. Nikolova, *SN Appl. Sci.*, **1**, 607 (2019); https://doi.org/10.1007/s42452-019-0592-3

3. J.K. Hedlund Orbeck and R.J. Hamers, *J. Vacuum Sci. Technol. A*, 38, 031001 (2020); https://doi.org/10.1116/1.5141853
4. A.M. Abu-Dief, *J. Nanotechnol. Nanomater.*, **1**, 5 (2020).
5. J.A. Rodriguez and M. Fernandez-Garcia, Synthesis, Properties and Applications of Oxide Nanoparticles, Wiley: New Jersey (2007).
6. M. Fernandez-Garcia, A. Martinez-Arias, J.C. Hanson and J.A. Rodriguez, *Chem. Rev.*, **104**, 4063 (2004); https://doi.org/10.1021/cr030032f
7. R. Medhi, M.D. Marquez, and T.R. Lee, *ACS Appl. Nano Mater.*, **3**, 6156 (2020); https://doi.org/10.1021/acsanm.0c01035
8. N. Millot, D. Aymes, F. Bernard, J.C. Niepce, A. Traverse, F. Bouree, B.L. Cheng and P. Perriat, *J. Phys. Chem. B*, **107**, 5740 (2003); https://doi.org/10.1021/jp022312p
9. J. Schoiswohl, G. Kresse, S. Surnev, M. Sock, M.G. Ramsey and F.P. Netzer, *Phys. Rev. Lett.*, **92**, 206103 (2004); https://doi.org/10.1103/PhysRevLett.92.206103
10. J.M. McHale, A. Auroux, A.J. Perrota and A. Navrotsky, *Science*, **277**, 788 (1997); https://doi.org/10.1126/science.277.5327.788
11. H. Zhang and J.F. Banfield, *J. Mater. Chem.*, **8**, 2073 (1998); https://doi.org/10.1039/a802619j
12. O.A. Oyewo, E.E. Elemike, D.C. Onwudiwe and M.S. Onyango, *Int. J. Biol. Macromol.*, **164**, 2477 (2020); https://doi.org/10.1016/j.ijbiomac.2020.08.074
13. S. Varzdar, L. Hashemi, A. Morsali and M. Dusek, *J. Iran. Chem. Soc.*, **14**, 2255 (2017); https://doi.org/10.1007/s13738-017-1162-5
14. P. Veluchamy, M. Sharon, M. Shimizu and H. Minoura, *J. Electroanal. Chem.*, **365**, 179 (1994); https://doi.org/10.1016/0022-0728(93)02973-L
15. S. Ghasemi, M.F. Mousavi, M. Shamsipur and H. Karami, *Ultrason. Sonochem.*, **15**, 448 (2008); https://doi.org/10.1016/j.ultsonch.2007.05.006
16. A. Miri, M. Sarani, A. Hashemzadeh, Z. Mardani and M. Darroud, *Green Chem. Lett. Rev.*, **11**, 567 (2018); https://doi.org/10.1080/17518253.2018.1547926
17. B. Jia and L. Gao, *Mater. Chem. Phys.*, **100**, 351 (2006); https://doi.org/10.1016/j.matchemphys.2006.01.012
18. S. Li, W. Yang, M. Chen, J. Gao, J. Kang and Y. Qi, *Mater. Chem. Phys.*, **90**, 262 (2005); https://doi.org/10.1016/j.matchemphys.2004.02.022
19. L.J. Chen, S.M. Zhang, Z.S. Wu, Z.J. Zhang and H.X. Dang, *Mater. Lett.*, **59**, 3119 (2005); https://doi.org/10.1016/j.matlet.2005.05.031
20. F.G. Ma, Z.Q. Shao, L.Y. Song and H.M. Tan, *Chin. J. Synth. Chem. (Hecheng Huaxue)*, **9**, 449 (2001).
21. Z.W. Pan, Z.R. Dai and Z.L. Wang, *Appl. Phys. Lett.*, **80**, 309 (2002); https://doi.org/10.1063/1.1432749
22. M. Ghaedi, A.M. Ghaedi, B. Mirtamizdoust, S. Agarwal and V.K. Gupta, *J. Mol. Liq.*, **213**, 48 (2016); https://doi.org/10.1016/j.molliq.2015.09.051
23. K.H.H. Al-Attiyah, A. Hashim and S.F. Obaid, *Int. J. Plast. Technol.*, **23**, 39 (2019); https://doi.org/10.1007/s12588-019-09228-5
24. L. Zhan, X. Xiang, B. Xie and B. Gao, *Powder Technol.*, **308**, 30 (2017); https://doi.org/10.1016/j.powtec.2016.12.005
25. S.G. Rejith and G. Sudha, *Int. Adv. Res. J. Sci. Eng. Technol.*, **4**, 130 (2017); https://doi.org/10.17148/IARJSET.2017.4230
26. P.B. Taunk, R. Das, D.P. Bisen and R. Tamrakar, *Optik*, **127**, 6028 (2016); https://doi.org/10.1016/j.ijleo.2016.04.073
27. M. Salavati-Niasari, F. Mohandes and F. Davar, *Polyhedron*, **28**, 2263 (2009); https://doi.org/10.1016/j.poly.2009.04.009
28. A. Ramazani, S. Hamidi and A. Morsali, *J. Mol. Liq.*, **157**, 73 (2010); https://doi.org/10.1016/j.molliq.2010.08.012
29. V.S. Kundu, R.L. Dhiman, D. Singh, A.S. Maan and S. Arora, *Int. J. Adv. Res. Sci. Eng.*, **2**, 5 (2013).
30. R.S. Dongre, eds.: P. Chooto, Lead: Toxicological Profile, Pollution Aspects and Remedial Solutions, In: Lead Chemistry, IntechOpen (2020).
31. R. Thielsch, T. Bohme, R. Reiche, D. Schlafer, H.D. Bauer and H. Bottcher, *Nano Struct. Mater.*, **10**, 131 (1998); https://doi.org/10.1016/S0965-9773(98)00056-7
32. T.J. Wilkinson, D.L. Perry, E. Spiller, P. Berdahl, S.E. Derenzo and M.J. Weber, *Proc. MRS*, **704**, 117 (2002).
33. P. Tyagi and A.G. Vedeshwar, *Bull. Mater. Sci.*, **24**, 297 (2001); https://doi.org/10.1007/BF02704925
34. D. Chu, Y. Zeng and D. Jiang, *Solid State Commun.*, **143**, 308 (2007); https://doi.org/10.1016/j.ssc.2007.05.036